Environment Canada Environnement Canada

National Hydrology Research Institute

NHRI PAPER NO. 15

Albedo Survey on Andrei Glacier, Iskut River Basin, B.C., Midsummer, 1980

S. Fogarasi

NHRI

NATIONAL HYDROLOGY RESEARCH INSTITUTE
INLAND WATERS DIRECTORATE
OTTAWA, CANADA, 1981

90-05386/

Contents

	Page
ABSTRACT	v
RÉSUMÉ	v
INTRODUCTION	1
GEOGRAPHIC SETTING	1
OBSERVATIONS	1
DATA ANALYSIS	6
CONCLUSION	9
ACKNOWLEDGMENTS	11
REFERENCES	11
APPENDIX. Use of the calibration factors	12

Tables

1.	Description of the observation sites	4
2.	Geary's statistics calculated for each albedo group	7
3.	Test of normality by means of the A and B parameters at the indicated probability levels	7
4.	The range of albedo variation at the indicated probability levels	9
5.	Mean albedo values along an 11 x 23 grid superimposed on Andrei Glacier	9

Illustrations

Figure 1.	Topography of Andrei Glacier and vicinity	2
Figure 2.	Portable albedo meter in resting position	3
Figure 3.	(a) All of the albedo measurements plotted against local time and (b) histogram of all of the albedo measurements taken in July and August of 1980 on Andrei Glacier	5
Figure 4.	Albedo measurements grouped in the function of ice surface contamination	6
Figure 5.	Frequency distribution of the four albedo groups with the scale of standard normal density function [$\phi(z)$]	8
Figure 6.	Estimation of the albedo class boundaries in terms of ice surface contamination over Andrei Glacier	10

Abstract

At nine sites on Andrei Glacier, B.C., albedo measurements were carried out on ice surfaces which were contaminated to varying degrees. Four albedo classes were derived in terms of the amount of aeolian dirt that was deposited on the ice surface. Each albedo class was associated with one of the "white," "whitish," "dirty" or "very dirty" surfaces, and each class had significantly different albedos, the means of which ranged from 22% to 68%.

Values in each albedo group were normally distributed over time. Albedos from wet ice surfaces were found between the -2 and -3 standard deviation band of each albedo class distribution. Albedo values measured on freshly frozen ice surfaces tended to occupy the upper tail of the Gaussian normal distribution, i.e., between +2 and +3 standard deviations.

Albedo values have been tabulated and plotted along a grid of 500-m mesh. Finally, suggestions are given on how to model hourly ice surface albedo distribution over the glacier.

Résumé

À neuf endroits sur le glacier Andrei, en Colombie-Britannique, on a mesuré l'albédo de surfaces glacées dont la contamination variait. Quatre classes d'albédo ont été obtenues en fonction de la quantité de poussières éoliennes déposées sur ces surfaces. Chaque classe était associée à l'une des surfaces suivantes: blanche, blanchâtre, salie, et très salie. Chacune des classes possédait des albédos significativement différents, dont la moyenne variait entre 22 % et 68 %.

Dans chaque groupe d'albédos, les valeurs étaient normalement distribuées en fonction du temps. Les albédos des surfaces glacées mouillées se situaient entre -2 et -3 écarts types de la distribution de chaque classe. Les albédos des surfaces fraîchement gelées occupaient plutôt l'autre extrême du spectre de Gauss de la distribution normale, c'est-à-dire entre +2 et +3 écarts types.

Les albédos ont été mis sous forme de tableaux et représentés graphiquement selon un quadrillage dont les carreaux avaient 500 m de côté. Enfin, on donne des conseils pour modéliser la répartition horaire de l'albédo sur le glacier.

Albedo Survey on Andrei Glacier, Iskut River Basin, B.C., Midsummer, 1980

S. Fogarasi

INTRODUCTION

This report is a contribution to the general water resource and geological survey of the Iskut River basin. The albedo survey and mapping were necessary because glacier albedo values are seldom recorded (on a regular basis) as part of the observation routine of weather stations. The knowledge of glacier surface albedo, however, is essential for the successful calculation of surface heat exchanges, glacier-melt predictions, and local energy budget.

When this albedo survey was made (July 18 to August 3, 1980), the accumulated snow in the measurement area had already melted. Only the end result of the snow metamorphism was visible during the observation period. Just a brief summary is given here concerning the possible evolution of the glacier surface. This summary is necessary because any stage of this evolution results in different albedo values for the observation period. The more or less porous glacier ice surface is made up of different granular sizes. The term used here for a cluster of decomposed ice crystals is "granular ice." The basic unit of surface ice, granula, even in a dry condition, is covered by water in an eight- to ten-molecule layer. When the surface air temperature increases and melt begins, three phases of water can be present in the surface: liquid, solid and vapour. During this evolution, the electrical, mechanical and optical properties of the ice surface change. Therefore it is expected that albedo values will vary and show a diurnal pattern during melting and refreezing.

As the snow melted, individual dirt particles, by absorbing more solar radiation than the ambient ice surface, sank into the ice by creating vertical hollow tubes 1–25 cm long. In late July, dirt particles were still visible on the bottom of the tubes. Accordingly, the glacier ice surface has been found to have sections ranging from "white" to "whitish" to "dirty" to "very dirty." The hollow tubes were occasionally found to be dry or filled with meltwater. It was assumed that a strong seasonal evolution had developed in surface albedo values as dirt settled deeper and deeper with the melting of the accumulated snow cover. As the dirtiness increased the albedo decreased. While shortwave absorption by dirt continued the amount of melt rate on the glacier surface increased.

The presence of surface meltwater might influence the diurnal radiation pattern. The deeper the streams were by mid-day on the glacier surface, the higher the shortwave absorption became. Meltwater helped to minimize horizontal albedo gradients over any specific spot of the glacier surface.

GEOGRAPHIC SETTING

Andrei Glacier is located in the Boundary Ranges of the Coast Mountains in British Columbia. The glacier extends in a west to east direction and the lower section is approximately 11 km long and 1.6–3.2 km wide. This ice tongue drains into Forrest Kerr Creek, a tributary of the Iskut River.

A 1: 50 000 scale map is shown of Forrest Kerr Creek, Cassiar Land District, B.C., on Surveys and Mapping Branch topographic sheets numbered 104 B/14 and 104 B/15. A section of this area with Andrei Glacier is presented in Figure 1.

OBSERVATIONS

Since strict budgetary aspects imposed financial restrictions on the fieldwork, the study was a one-man operation. Therefore field instruments had to be light, portable and self-levelling. The self-levelling bracket holding the instrument was designed and built in-house. For measurements, a Kipp & Zonen pyranometer was used; it had been calibrated by the Radiation Instruments Calibration Section of the Atmospheric Environment Service of Environment Canada in Toronto (May 10, 1980). The calibration certificate and the use of the calibration factors are documented in the Appendix. The pyranometer was sensitive to radiation with a wavelength band of 0.3–2.5 μm. Calibration of the pyranometer was done at 25°C temperature, producing a -0.00139/°C temperature coefficient. To obtain the absolute temperature difference between 25°C and the screen temperature, air temperatures were measured with a sling thermometer. The self-levelling bracket which holds the instrument was attached to telescoping aluminum tubing, 2.5 m long; a millivoltmeter was connected to the sensor through the end

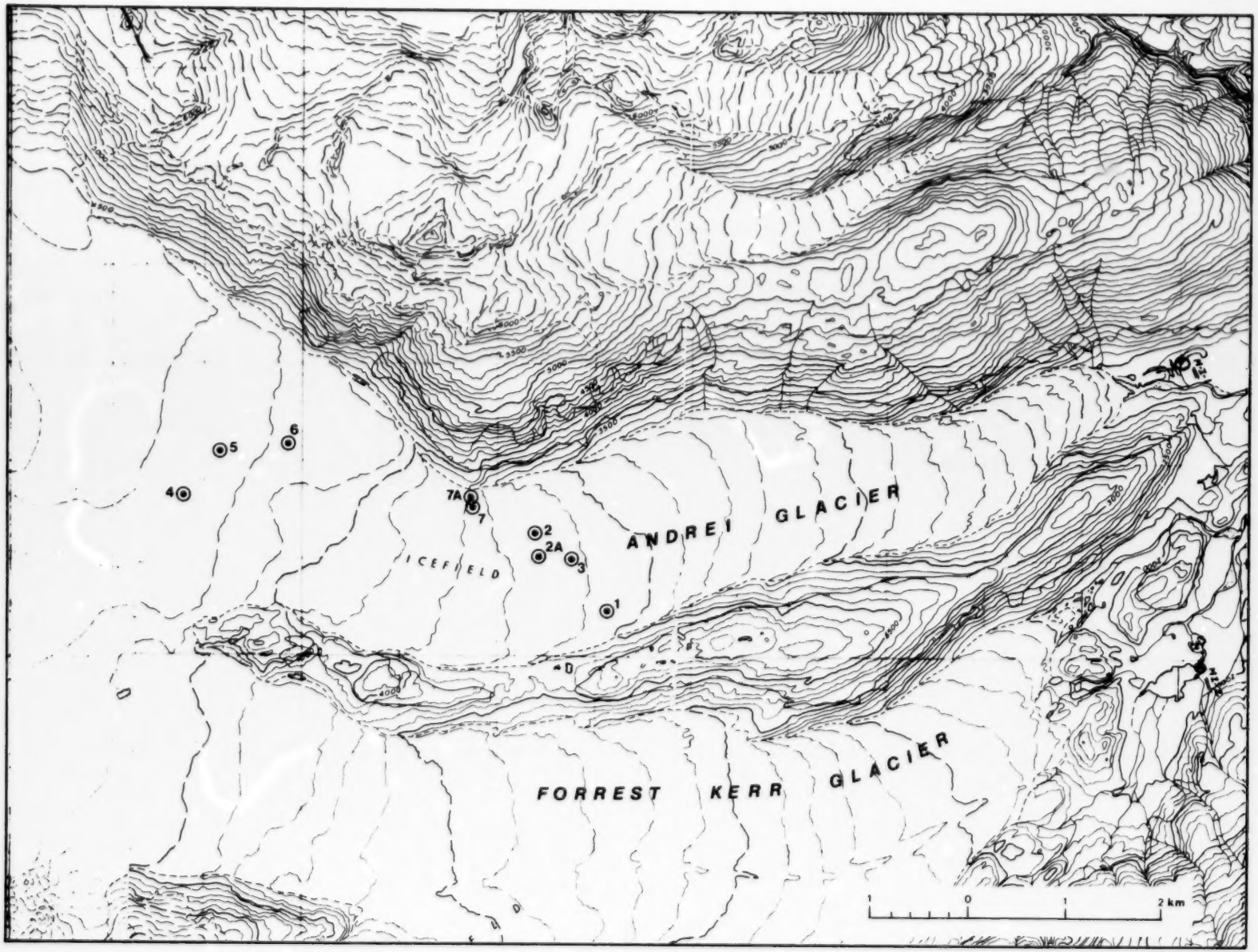

Figure 1. Topography of Andrei Glacier and vicinity.

of this metal tube. For the voltmeter, a portable 9-V battery-operated Data Precision Digital Multimeter (model 2584 1/2-DMM) was used. The instrument was first designed as a hand-held portable device. It proved to be too unstable, however, and the handle, 2.5 m long, was placed on a photographic tripod, 1 m high, to eliminate hand-held vibrations. The instrument setup, in a resting position, is shown in Figure 2. The telescoping pole was never attached to the tripod, and during observation the pyranometer was placed forward and the black-coloured section of the pole was shifted forward over the tripod attachment. While not in use (Fig. 2) in this resting position, moderate wind could not overturn it.

Figure 2. Portable albedo meter in resting position.

As the first step, the down-coming shortwave radiation, R_D, was measured by turning the glass dome of the pyranometer upward. The response time was approximately 15 s. After this 15-s exposure, the R_D value was read off and the handle was turned upside down by pointing the glass dome downward and measuring the value of the upward reflection, R_U. The term "albedo," α, as it is used here, means both the surface reflection and the outcoming portion of the scattering that was generated within the snow cover. The albedo was calculated with a well-known formula (Arai, 1966),

$$\alpha = R_U/R_D$$

where R_U depends on the physical properties of the surface.

Observations were done as frequently as possible, occasionally at every 15-min interval when the weather conditions permitted. Due to rainy weather conditions there were no observations made on July 19, 22, 29 and 31, 1980.

Although the instrumentation was light and easy to handle, there were some disadvantages. For example, the presence of the observer and the tripod contaminated the radiation field. To reduce these errors, the observer stood up when the R_U components were measured and bent down when the R_D components were measured. These errors would not have been eliminated if the albedo meter had been attached to an instrumentation tower. Of course, this latter system could not have been used in this case because it is not portable and the presence of the tower would contaminate the radiation field. The other disadvantage in measuring albedo with a single pyranometer is apparent when stratocumulus or cumulus clouds shade the sun. During the 15-s response time, sky condition frequently changed and the readings could not be stabilized. Or, if they could be stabilized, when turning the handle down-position for another 15 s to measure the R_U component, the sky condition would change again. Readings of R_U and R_D in these cases indicated two different sky conditions. Therefore, these values were discarded because they were unrelated. When the cloud cover ranged between 7/10 and 10/10 or clear sky prevailed, the albedo measurements were easy to take. But in the case of a transparent stratocumulus or cumulus cloud cover, the observer frequently had to wait 1 to 1.5 h before a single measurement could be accomplished. In most cases, the sky conditions were overcast.

Slope and aspect were measured at each site with an inclinometer and a magnetic compass by using 30°E magnetic correction to obtain true aspects. For the determination of slope and aspect, the general character of the glacier surface was measured around the observation point rather than right under the glass dome of the pyranometer. The assumption was made that reflection from every direction influenced the value of R_U. Occasionally, when the general slope of the adjacent surface and the slope of the site were identical, the orientation of the slope was determined by the direction of motion of a rolling ball.

As reported by Petzold (1977), at higher than 40° solar elevation the height of sun had no influence on albedo. During the observation period the highest slope angle that was measured never exceeded 5°. Due to logistic and manpower problems, observations could not take place before 09:00 a.m. PDT. After 09:00 a.m., the elevation of the sun and the angle of incidence were higher than 40°. The lack of early observation could not cause major problems because the initial objective was to plot the horizontal albedo distribution on Andrei Glacier. On some of the Western Cordilleran glaciers, one observation was performed for each climatological variable daily. On most of the glaciers, however, no climatological observations were ever done. At higher than 40° solar elevation, no diurnal albedo pattern existed; hence noon albedo could be

considered representative of the average albedo conditions at each site. Previously, in their albedo-change models, Petzold (1977) and Fogarasi (1980) used only noon albedo values as input into some of the reputable radiation models. These models were described earlier by Davis (1979), Garnier (1968), Garnier and Ohmura (1968), Hay (1971, 1976, 1977) and Hay and Suckling (1977). They can utilize and modify the noon albedo values according to the hourly changes in solar elevations, topographic slopes and aspects.

The slope and aspect observations were traditionally done and their values were recorded. However, their analysis ended inconclusively, that is, no relationship was found between albedo and solar elevation. Therefore no further discussion will be given on this subject.

The texture of the glacier surface at the sites was observed and grain size was visually estimated. It was determined whether each site was dry, wet or overflown by water, and the degree of its dirtiness was also estimated. Finally, the dominant cloud types, their amounts and the total cloud cover were also observed. The effect of cloud condition on the albedo values was undetected by the ensuing analysis, as most of the time overcast conditions prevailed.

The main problem of performing the albedo survey on Andrei Glacier involved the sampling technique or site selection for observation. With only one observer it was difficult or even impossible to measure albedo along a grid network several times a day to find out whether any diurnal pattern existed or not. Walking in many parts of the glacier was extremely difficult and hazardous. The glacier was full of deep crevasses which were frequently covered with a thin layer of snow. With respect to this difficulty, the only possible alternative was to measure and analyze albedo values in terms of the reddish dirt found on the glacier surface. Therefore identical appearances of the red sediments over the glacier surface were subjectively chosen from the air, and the observation spots were selected within each class of a recognizable red tone. This sampling scheme is known as a stratified method of sampling, and it is generally accepted as an efficient approach. Nine sites were considered for observation on the basis of their appearance and accessibility. The locations of these spots are indicated in Figure 1. Observations on these sites were done within a 300-m diameter. The instrument was shifted within this area each day because the natural surface was disturbed during a couple of hours of observation. The characteristics of the observation sites are described in Table 1.

Table 1. Description of the Observation Sites

Site No.	Grain size	Appearance of site	Appearance of area around site
1	1.5–5.0 cm	Very dirty original surface	Entire surface very dirty and cut by crevasses, 0.2–1.5 m wide
	1.0–2.0 cm	The very dirty surface transformed into bluish white ice	
2,2A	3.0–4.0 mm	Dirty frozen porous snow	Whitish-bluish hummocky surface with dirty spots; many puddles and streams
3	3.0–4.0 mm	Dirty spots in bluish-white frozen porous snow surface	Slightly dirty surface and many streams, 15–20 cm deep
4	1.0–2.0 mm	Slushy, wet bluish-white snow	Slushy, wet snow-fill patches in bluish ice-hollows and crevasses
	3.0–4.0 mm	Bluish bare frozen snow	
5	1.0–2.0 mm	White slushy, wet snow	White, slightly bluish; 20% of the bluish ice area is covered with crevasse snow-fill
	2.0–3.0 mm	Frozen porous bluish snow	
6	0.5–1.0 mm	White wet snow patches	Crevasse snow-fill and bluish water puddles
7,7A	3.0–5.0 mm	Whitish porous frozen snow	Whitish hummocky area with many bluish water puddles

Two different surfaces are described for site No. 1. The two contamination domains on site No. 1 suggest that these surfaces are in continuous change, namely, within a very dirty area bright spots may develop. Dirt and debris sink into the ice so deeply that the debris is no longer visible. Only the relics of this evolution process remained on the surface in the form of porous frozen snow with a granular size of 1-2 cm. From site No. 1 observations were done on both the very dirty and the bright spots undergoing transformation. (One was classified as very dirty and the other, as dirty.) Sites Nos. 2 and 2A were located on either side of the boundary line of a dirty and a whitish section. Site No. 2 is in the whitish zone and No. 2A is in the dirty zone. This area was frequently covered with a sheetwash type of surface flow. In the afternoon, the albedo values from these sites frequently were similar because of the high water content at both sites. Site No. 3 is located on a ridge of the glacier within the dirty section and entrenched by many small streams. Site No. 4 is in the white section. Site No. 5 is a representative spot for the whitish zone, but 20% of its area is covered with white slushy snow-fill. Site No. 6 and its vicinity appear whitish because its dirty bluish ice surface is spotted with slushy snow-fill and many water puddles. Owing to this water, the zone

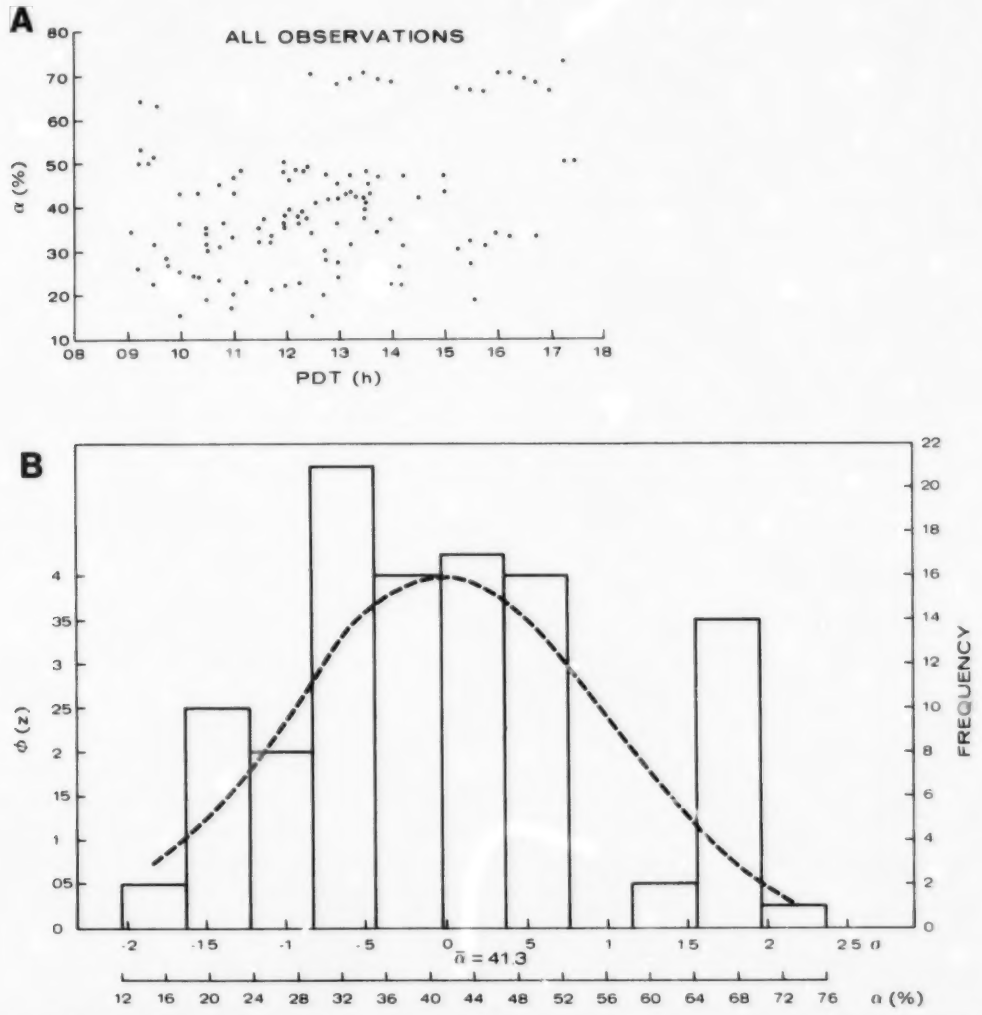

Figure 3. *A* – All of the albedo measurements plotted against local time and *B* – histogram of all of the albedo measurements taken in July and August of 1980 on Andrei Glacier.

appears as an area of uniform brightness. Sites Nos. 7 and 7A are located at the boundary between the dirty and very dirty zones with newly transformed whitish surfaces.

DATA ANALYSIS

All of the albedo values measured were plotted against the time of observation in PDT (Fig. 3A). The cluster of dots does not show much regularity (Fig. 3B). Next, the albedo values were grouped into contamination categories, which are shown in Figure 4.Variations within the albedo categories are slight. Within the very dirty group at 10:05 a.m. PDT, the $\alpha = 15\%$ value was due to sheetwash that had occurred on the previous day. Sheetwash had loosened chunks of grains, which made the surface very rough; walking on this surface was like walking on ball bearings. Hence the albedo was low. On the following day cracks were filled with meltwater which later froze. Thus, the albedo increased when the surface cracks were filled in and refrozen. The rest of the albedo classes did not show much variation. In fact, all of the values of each class appeared to scatter along a straight line.

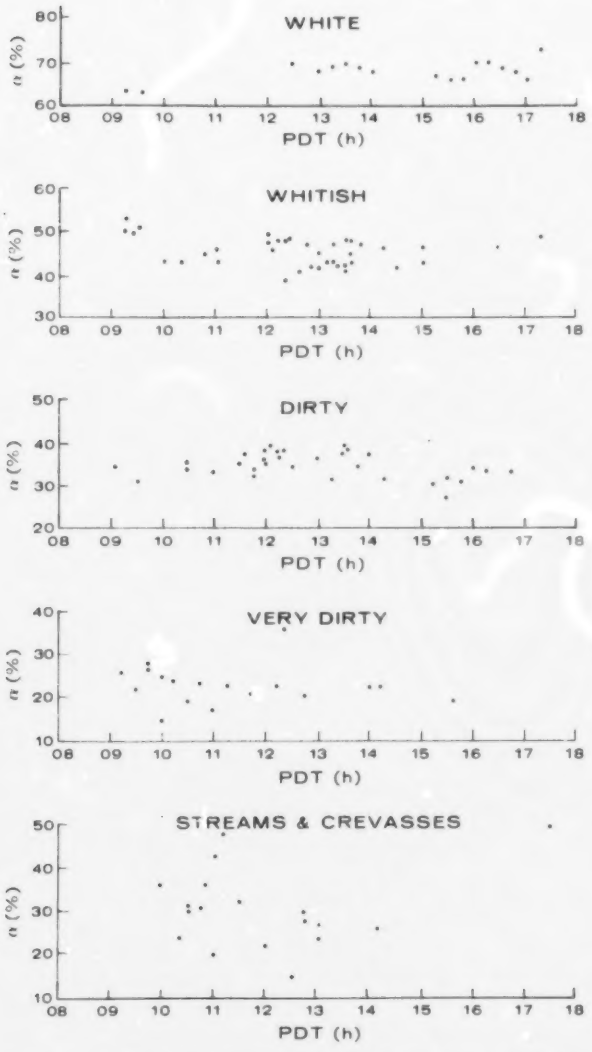

Figure 4. Albedo measurements grouped in the function of ice surface contamination.

The diagram of streams and crevasses (Fig. 4), however, shows a wide scatter of values. Albedo measurements over deep crevasses indicated no relevance to albedo values measured over the adjacent surface. Crevasse albedos appeared low at high solar elevation and appeared high at low solar elevation. When one side of a crevasse was illuminated, high reflection was observed. Albedos over shallow streams were measured at 75 cm above the water surface to minimize the environmental effect. Apparently, as shown by the wide scatter of dots, the influence of the ambient albedo field was not eliminated. None of these values, of course, was included in any of the albedo groups.

Next, the appearance of the normality of data was tested by using numerical evaluation. Following the studies of monthly precipitation by Kendall (1960) and Stidd (1953), in this albedo survey the measured albedo values were considered random samples. Now, if it is possible to prove that the albedo values are normally distributed, then the probability of albedos from wet or dry surfaces can be found from normal probability tables. Before attempting this, however, the normality of distribution is tested.

If the size of the sample is greater than 50–100, the χ^2 test can be applied to grouped frequencies to determine whether the values are within the Gaussian normal curve (Pearson *et al.*, 1936). The χ^2 test only takes into account the magnitude of the differences between observed and expected group frequencies and not their sign and arrangement. Our sample size ranged between 17 and 37; hence the χ^2 method could not be used for testing the normality of distribution. Instead, following the investigations of Kendall (1960), two parameters were used to detect normality:

(1) Geary's alternative statistic (A), which detects changes in kurtosis, and
(2) the third moment ratio (B), which reflects the magnitude of skewness.

The formulas for these parameters are:

$$A = \frac{\sum_{i}^{n'} |\alpha_i - \bar{\alpha}|}{\left\{ n' \sum_{i}^{n'} (\alpha_i - \bar{\alpha})^2 \right\}^{1/2}}$$

$$B = \frac{\sum_{i}^{n} (\alpha_i - \bar{\alpha})^3}{n S^3}$$

where $n' = n + 1$

For Gaussian normal distribution these statistics are given in Biometrika Tables (Pearson *et al.*, 1936; Pearson and Hartley, 1962). The relevant statistics, the A and B values, were calculated for each albedo class and are listed in Table 2. The upper and lower limits of the Geary's ratio (A) and the skewness (B) for Gaussian distribution are compiled from Biometrika Tables and are shown in Table 3. The observed values of B (the measure of skewness of the empirical distribution) fall within the upper and lower bounds for even as low as 80% limits. Thus, it can be concluded that the data are not significantly skew. Also, almost all the values of A (the kurtosis, i.e., the measure of the flatness of the tails of the empirical distribution) fall within the upper and lower bounds. The only exception is the .8609 kurtosis measure for a whitish surface, and this is only marginally significant at the 90% level.

Graphically, equal vertical scale was chosen for each normal curve. This is the reason that Figures 5B, 5C and 5D appear platykurtic ($B < 3$), Figure 5A seems to be normal ($B = 3$), and none of them appears leptokurtic ($B > 3$). In fact, Table 2 indicates that none of the kurtosis values reached 3, which is the ideal value for a normal Gaussian curve. But considering the small size of samples, as explained previously, the kurtosis values that are shown in Table 2 are not representative of the real kurtosis characteristics of the samples concerned. This is the reason that Geary's statistic (A) was used in this analysis rather than the kurtosis values.

Table 2. Geary's Statistics Calculated for Each Albedo Group

Albedo class	No. of cases	A	B	Kurtosis	Mean	Standard deviation (S)
White	17	0.7606	-0.2295	2.8711	68	2.5
Whitish	37	0.8609	-0.1128	2.0688	45.2	3.4
Dirty	33	0.8004	-0.3616	2.8285	34.4	2.8
Very dirty	17	0.7391	-0.1942	2.6219	22.1	3.4

Table 3. Test of Normality by Means of the A and B Parameters at the Indicated Probability Levels

Albedo class	Percentage point of distribution	A		B		Percentage of albedo values within these limits
		Lower	Upper	Lower	Upper	
White	1	.6829	.9137	-1.1	+1.1	98
	5	.7236	.8884	-.8	+.8	90
	10	.7452	.8733			80
Whitish	1	.7167	.8769	-.92	+.92	98
	5	.7440	.8578	-.62	+.62	90
	10	.7583	.8468			80
Dirty	1	.7167	.8769	-.92	+.92	98
	5	.7440	.8578	-.62	+.62	90
	10	.7583	.8468			80
Very dirty	1	.6829	.9137	-1.1	+1.1	98
	5	.7236	.8884	-.8	+.8	90
	10	.7452	.8733			80

Hence one can state with confidence that the albedo values within each class are not significantly abnormally distributed. Because of the symmetrical distribution about the mean values it is now possible to give the range of albedo variation (for each group), for example, with 80% to 98% probability. The variation of albedo is shown in Table 4. Because of the normality, there is a 95% probability that the actual albedo values can deviate only 2 standard deviation about the arithmetic mean, that is, $P((\bar{\alpha} - 2\sigma) \leqslant \alpha \leqslant (\bar{\alpha} + 2\sigma)) = .95$.

As described earlier, the solarimeter was placed 1 m above the surface. Therefore small ice morphologic features directly under the sensor could influence reflection values within a 2 standard deviation bound. It is believed that the 2 standard deviation band within each albedo class was at least partially produced by the variable reflections from the small ice morphologic features.

The frequency distribution of each albedo class is shown in Figure 5 where the curves of the normal density functions are superimposed. This figure reveals that only the dirty albedo class is overlapped with its two neighbours. This overlap was produced when meltwater covered the boundaries of dirty zones, diminishing the differences toward very dirty and whitish zones.

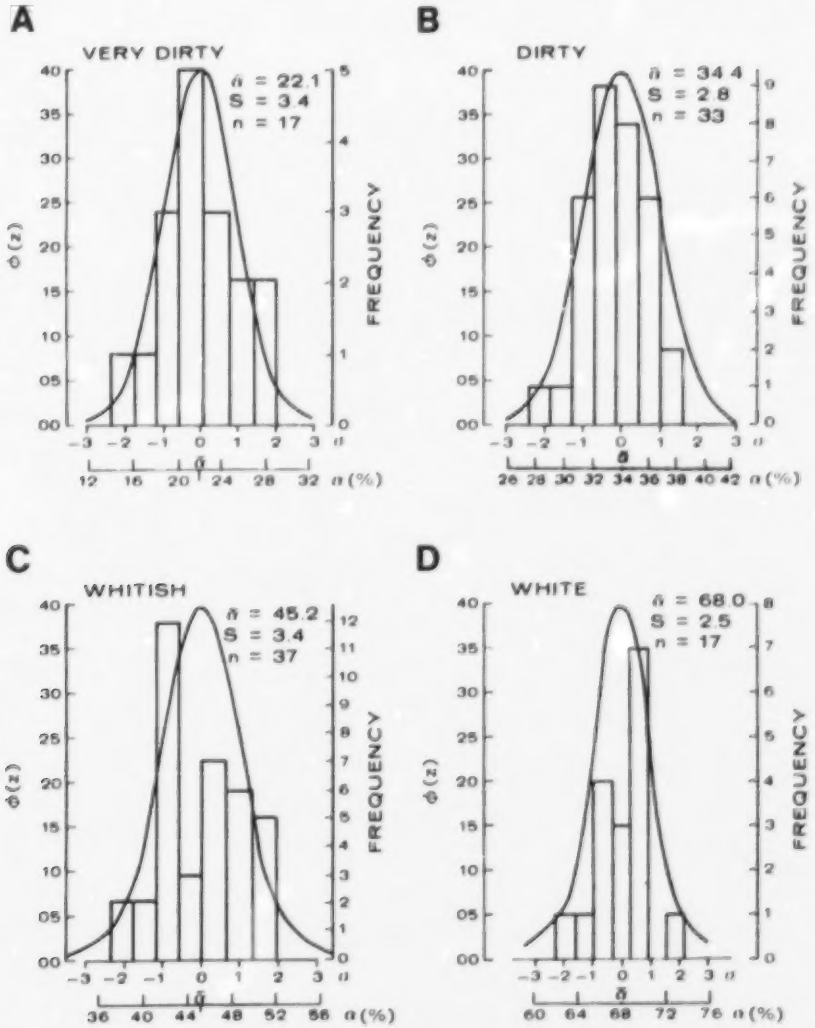

Figure 5. Frequency distribution of the four albedo groups with the scale of standard normal density function [$\phi(z)$].

Table 4. The Range of Albedo Variation at the Indicated Probability Levels

Albedo class	Range of albedo variation from 80% to 98% probability level
Very dirty	$P(18 \leq a \leq 26) = 80$
	$P(17 \leq a \leq 28) = 90$
	$P(15 \leq a \leq 29) = 96$
	$P(14 \leq a \leq 30) = 98$
Dirty	$P(31 \leq a \leq 38) = 80$
	$P(30 \leq a \leq 39) = 90$
	$P(29 \leq a \leq 40) = 96$
	$P(28 \leq a \leq 41) = 98$
Whitish	$P(41 \leq a \leq 50) = 80$
	$P(40 \leq a \leq 51) = 90$
	$P(38 \leq a \leq 52) = 96$
	$P(37 \leq a \leq 53) = 98$
White	$P(65 \leq a \leq 71) = 80$
	$P(64 \leq a \leq 72) = 90$
	$P(63 \leq a \leq 73) = 96$
	$P(63 \leq a \leq 74) = 98$

On the basis of the foregoing discussion, it can be said with confidence that the arithmetic means of these albedo groups represent reflections from the actual surfaces in terms of the reddish aeolian sediment deposited by snowdrifts. If the reddish contamination of the ice surface can be plotted, the numerical albedo distribution over the glacier surface can also be attempted.

It has not yet been pointed out that occasionally colour changes were gradual. This might cause an important problem in the classification procedure. These zones, however, were narrow strips and not sampled; only clearly defined areas were examined. Moreover, these intermediate narrow surfaces could not have been plotted on a topographic map due to scale consideration.

To estimate the lateral distribution of albedo on Andrei Glacier, five sideview colour photographs were used in identifying the degree of contamination over the glacier surface. This identification was performed on the basis of the actual measurements at nine sites. These nine sites were located on the photographs. Traverse lines connecting the outstanding topographic features were plotted on these colour images and then the traverse lines were transferred onto the topographic map. The locations of colour changes were tac-marked along the traverse lines and proportionally transferred onto the topographic sheet. The iso-tac marks were connected, and each albedo group was delineated on the topographic map. The contamination boundaries are shown as albedo classes in Figure 6. An 11 x 23 grid with a mesh size of 500 m is superimposed on this map. Albedo values were estimated for each grid point from the mean values in Table 2. The spatial variation in albedo is shown in Table 5. For the calculation of net radiation or energy budget distribution over the glacier surface, this table can prove a valuable tool.

CONCLUSION

Inspection of Figure 4 (showing the scatter of albedo values in function of time) revealed that morning albedo fluctuations were high over whitish and very dirty surfaces because sometimes they were dry and at other times wet.

White and dirty surfaces did not show morning fluctuations like the other two groups. This was, in part, because by the time the observer reached the middle part of the glacier where these two groups were measured, the morning frost was always gone and the ice surface was glazed with water. It should be noted that these sites were located over undulating hummocky surfaces. Albedo measurement in a wet depression during the day resulted in lower values than the measurements made on dry elevated spots. But the actual observations indicated a mean albedo of these two

Table 5. Mean Albedo Values Along an 11 x 23 Grid (mesh size of 500 m) Superimposed on Andrei Glacier.

	1	2	3	4	5	6	7	8	9	10	11	12	13	14	15	16	17	18	19	20	21	22	23
1	45	22	–	–	–	–	–	–	–	–	–	–	–	–	–	–	–	–	–	–	–	–	–
2	45	34	–	–	–	–	–	–	–	–	–	–	–	–	–	–	–	–	–	–	–	–	–
3	45	45	34	22	–	–	–	–	–	–	–	–	–	–	–	–	–	–	–	–	–	–	–
4	68	45	45	34	22	22	–	–	–	–	–	–	–	–	–	–	–	–	–	–	–	–	–
5	68	68	45	45	34	22	22	–	–	–	–	–	–	–	–	–	–	–	–	–	–	–	–
6	68	68	68	45	45	34	22	22	–	–	–	–	–	–	22	22	22	–	–	22	22	22	22
7	68	68	68	68	45	45	34	34	22	–	–	–	22	22	34	34	34	34	22	22	34	22	–
8	68	68	68	68	68	45	34	45	34	34	22	34	34	34	34	45	34	22	22	22	22	–	–
9	68	68	68	68	68	45	45	45	34	45	34	45	45	45	45	34	22	–	–	–	–	–	–
10	–	–	–	–	22	22	22	22	34	34	45	45	34	22	–	–	–	–	–	–	–	–	–
11	–	–	–	–	–	–	–	–	22	22	22	22	–	–	–	–	–	–	–	–	–	–	–

Note: Dashes indicate grid point locations outside the glacier.

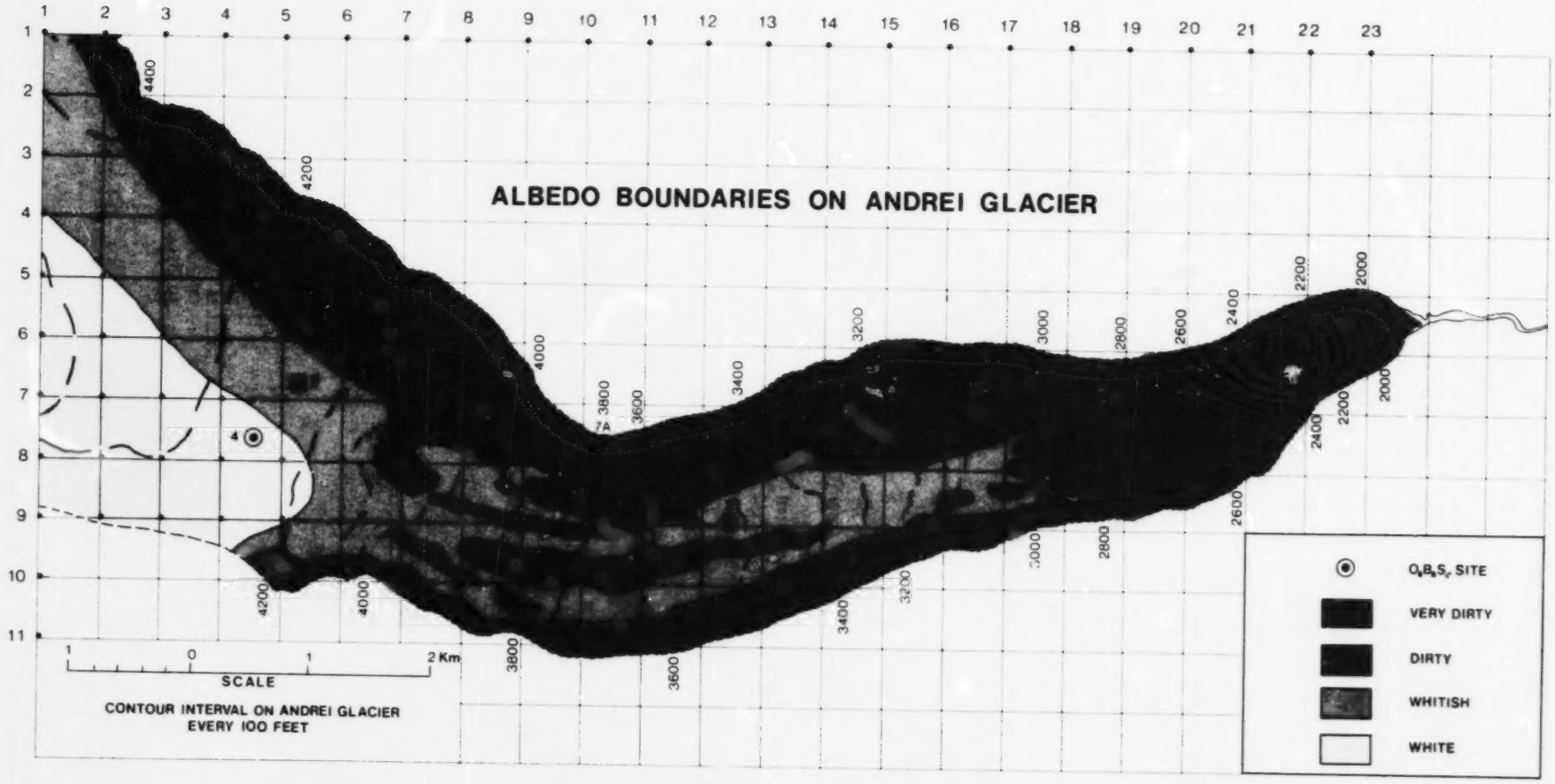

Figure 6. Estimation of the albedo class boundaries in terms of ice surface contamination over Andrei Glacier.

micro features at a 1-m height above the average surface. The exclusive influences from wet and frozen surfaces were equalized at this height.

Inspection of the raw data from each site revealed that values observed on extremely wet and dry refrozen surfaces fell in the lower or upper tail sections of the normal curves of Figure 5 from -2 to -3 and +2 to +3 standard deviations. There is no evidence of major albedo variation after 5 p.m. PDT. By accepting the normality and the symmetry of raw data for each albedo group, however, the recurrence of morning variation can be assumed for the evening.

Albedo distribution over Andrei Glacier can be modelled for all of the grid points shown in Figure 6, provided that the wetness of surface is known. If rain fell during the night or same day, one could predict wet albedos (that is, albedo values between -2σ and -3σ) from early morning to sunset. During a dry day, albedo values at the respective grid points remained between values of -2σ and $+2\sigma$. A computer program can be written in which the albedo values may be randomly generated within the appropriate standard deviation bounds for both wet and dry frozen conditions. Randomization is suggested because the multitude of micro features on the ice surface influences the site readings. The normal distribution of α values was explained with a single variable, dirtiness. This single variable could result in a linear or curvilinear relationship unless dirtiness was normally distributed as well. There were three more characteristics that could modify albedo values: shape, granular composition, and wetness of the micro features. Obviously, these three factors included in dirtiness were the causes of normal distribution of α values, and hence they were also normally distributed.

ACKNOWLEDGMENTS

The author would like to thank E.H. Burgess and T.W. Maxin, National Hydrology Research Institute, Environment Canada, for designing and building the instrument; L. Davies, B.C. Hydro, for his full support of the fieldwork operation and all personnel of the B.C. Hydro's Bob Quinn Lake Camp for their assistance and logistic support; O. Mokievsky-Zubok, National Hydrology Research Institute, for his generous guidance throughout the fieldwork operation; and Dr. P. Cohen, Computing and Applied Statistics Directorate, Environment Canada, for his valuable comments.

REFERENCES

Arai, T. 1966. On the relationship between albedo and the properties of snow cover. Jap. Prog. Climatol., pp. 88–95.

Davis, R.L. 1979. A computer program to map the spatial distribution of "clear sky" solar radiation in the Okanagan Valley of British Columbia. Paper presented at the 13th Annual Congress of the Canadian Meteorological and Oceanographic Society, May 30 – June 1, 1979, Victoria, B.C.

Fogarasi, S. 1980. A Preliminary Computer Program to Calculate Snow Surface Albedo Changes over Sentinel Glacier, B.C. Environment Canada, National Hydrology Research Institute, Progress Report, February 1980.

Garnier, B.J. 1968. Estimating the topographic variation of direct solar radiation: a contribution to geographical microclimatology. Can. Geogr. XII(4): 241–248.

Garnier, B.J. and A. Ohmura. 1968. A method of calculating the direct shortwave radiation income of slopes. J. Appl. Meteorol. 7: 796–800.

Hay, J.E. 1971. Computational model for radiative fluxes. J. Hydrol. (N.Z.), 10: 36–48.

Hay, J.E. 1976. A revised method for determining the direct and diffuse components of the total shortwave radiation. Atmosphere, 14(4): 278–287.

Hay, J.E. 1977. Shortwave Radiation on Inclined Surfaces. Report to Atmospheric Environment Service, Toronto, Contract No. DSS 05576-02095, August 1977.

Hay, J.E. and P.W. Suckling. 1977. Problems associated with the determination of solar radiation fluxes in the Cordilleran area of Western Canada. R.W. Longley Volume, Division of Meteorology, University of Alberta.

Kendall, G.R. 1960. The cube-root-normal distribution applied to Canadian monthly rainfall totals. International Association of Scientific Hydrology Conferences, Helsinki, No. 53, pp. 250–260.

Pearson, K. and H.O. Hartley, eds. 1962. *Biometrika Tables for Statisticians*. 2nd ed., University Press, Cambridge, Vol. 1, pp. 61–63 and 183–184.

Pearson, K., E. Pearson and G.M. Morant, eds. 1936. *Biometrika*. 1st ed., University Press, Cambridge, Vol. 28, pp. 304–307.

Petzold, D.E. 1977. An estimation technique for snow surface albedo. Climatological Bulletin, No. 21, McGill University, pp. 1–11.

Stidd, C.K. 1953. Cube-root-normal precipitation distributions. Trans. Am. Geophys. Union, 34(1): 31–35.

APPENDIX

USE OF THE CALIBRATION FACTORS

The instrument calibration certificate obtained for this study is presented in Figure A-1.

The following is an example illustrating the use of the calibration factors. On July 18, 1980, at 09:05 a.m. PDT, the following observations were made at site No. 1:

R_U mV = 5.46 mV

R_D mV = 1.73 mV

Screen temperature, T = 4.5°C

$$\text{Calibration factor} = \frac{1 \text{ cal}}{7.71 \text{ mV cm}^2 \text{ min}}$$

The solution would be:

ΔT = Temperature difference = $|T°C - 25°C|$

$= |4.5°C - 25°C| = 20.5°C$

$$R_U = \frac{5.46 \text{ cal}}{7.71 \text{ cm}^2 \text{ min}} - (\Delta T \times (-0.00139/°C))$$

$= 0.7081712 \text{ cal/cm}^2 \text{ min} + 0.28139$

$= 0.73666 \text{ cal/cm}^2 \text{ min}$

$R_U = 0.7366 \text{ langley/min} = 513.673 \text{ W/m}^2$

$= 0.030834076 \text{ MJ/m}^2 \text{ min}$

Similarly for R_D,

$$R_D = \frac{1.73 \text{ cal}}{7.71 \text{ cm}^2 \text{ min}} + 0.28139 = 0.252878 \text{ cal/cm}^2 \text{ min}$$

$R_D = 0.252878 \text{ langley/min} = 176.331 \text{ W/m}^2$

$= 0.010585473 \text{ MJ/m}^2 \text{ min}$

$$\alpha = \frac{R_D}{R_U} = .3432$$

$\therefore \alpha = 34\%$

Environment Canada
Atmospheric Environment

Environnement Canada
Environnement Atmospherique

NATIONAL ATMOSPHERIC RADIATION CENTRE

Calibration Certificate No. 80-16

Type of Radiometer Pyranometer

Manufacturer Kipp & Zonen

Model Number CM-5

Serial Number 72-1616

Calibration Factor, Short-Wave 11.06 $\mu V\ W^{-1}\ m^2$ = 7.71 $mV/cal\ cm^{-2}\ min^{-1}$

Calibration Factor, Long-Wave

Temperature of Calibration 25°C

Temperature Coefficient -0.00139/°C (Assigned)

Internal Resistance

Remarks Certificate expires 10 May 1982.

In Charge of Test

Approved

for **Assistant Deputy Minister**

Date of Approval 13 5 81

NOTES: a. Short-Wave calibration factors are based on the International Pyrheliometric Scale 1956. (Smithsonian scale of 1913 reduced by 2.0%)

b. 1 langley min^{-1} = 1 Calorie $cm^{-2}\ min^{-1}$
= 697.3 $W\ m^{-2}$
= 221 BTU $ft^{-2}\ hr^{-1}$

Figure A-1. Instrument calibration certificate.